# Principles governing recruitment of motoneurons during swimming in zebrafish

Jens Peter Gabriel, Jessica Ausborn, Konstantinos Ampatzis, Riyadh Mahmood, Emma Eklof-Ljunggren, Abdel El Manira

**Principles governing recruitment of motoneurons during swimming in zebrafish**

Jens Peter Gabriel#*, Jessica Ausborn*, Konstantinos Ampatzis, Riyadh Mahmood, Emma Eklöf-Ljunggren and Abdeljabbar El Manira

Department of Neuroscience, Karolinska Institutet, 171 77 Stockholm, Sweden

*These authors contributed equally to this study.

#Present address: Max Planck Institute for Medical Research, 69120 Heidelberg, Germany

Corresponding author: Abdel El Manira, Department of Neuroscience, Karolinska Institutet, SE-171 77 Stockholm, Sweden.

Tel: +46 8 524 6911, Fax: +46 8 349544, E-mail: Abdel.ElManira@ki.se

**Abstract**

Locomotor movements are coordinated by a network of neurons that produces sequential muscle activation. Different motoneurons need to be recruited in an orderly manner to generate movement with appropriate speed and force. However, the mechanisms governing the recruitment order have not been fully clarified. Here we show, using an *in vitro* juvenile/adult zebrafish brainstem-spinal cord preparation, that motoneurons are organized in four pools with specific topographic locations and are incrementally recruited to produce swimming at different frequencies. The threshold of recruitment is not dictated by the input resistance of motoneurons but is rather set by a combination of specific biophysical properties and the strength of the synaptic currents. Thus, our results provide insights into the cellular and synaptic computations governing recruitment of motoneurons during locomotion.

## Introduction

Motor behaviors emerge from the coordinated activity of neural circuits that produce a sequential activation of muscles. Motoneurons represent the final stage of neuronal processing; they thus need to be recruited in an orderly fashion to produce coordinated movement with the appropriate strength to meet the behavioral demand. The "size principle" describes the sequence of recruitment of motor units to produce movement with increased force or speed [1-5]. Classically, the order of recruitment of motoneurons was considered to depend on the input resistance where small motoneurons with high input resistance reach threshold before large ones with low input resistance [4-6]. This assumes that the threshold and the synaptic inputs are uniformly distributed among different motoneurons [1, 4, 5, 7, 8]. There exist appreciable differences in the excitability of motoneurons that are, to a large extent, unrelated to motoneurons size [9, 10]. Much has been learned about the orderly recruitment of motor units, but the specific cellular and synaptic properties setting the recruitment threshold of motoneurons have been difficult to unravel.

Recently, it was shown in larval zebrafish that motoneurons and interneurons follow specific rules of recruitment. The pattern of motoneuron recruitment at different swimming frequencies follows the size principle [11]. Small, high resistance motoneurons are activated at low frequencies with progressive addition of large, low resistance ones at higher frequencies. Unlike motoneurons, there is a continuous shift of the active set of interneurons at different swimming frequencies [12, 13]. The recruitment of interneurons at faster speeds is accompanied by the silencing of those driving movements at slower speeds [13-15]. In zebrafish, motoneurons develop along the dorso-ventral axis with the early born, large primary motoneurons located dorsally and later born, small secondary motoneurons located ventrally [16-19]. At early developmental stages, zebrafish larvae swim in bursts and only embryonic muscle fibers are developed [20-22]. At later stages of development there is a slow increase in number of adult red

(slow) muscle fibers that start to appear after two weeks post-hatching [22]. This is correlated with a change from burst swimming to the adult pattern of slow, steady swimming movements with continuously active red musculature [23-25]. Given the developmental maturation of motoneurons, muscle fibers and swimming pattern, it is possible that rules governing the recruitment of motoneurons are also adapted to meet the changes in swimming pattern and frequency as the zebrafish grows towards adulthood.

Here we investigate the principles governing the recruitment of motoneurons during swimming in juvenile/adult zebrafish. We show that motoneurons are organized in four pools with specific topographic locations and are incrementally recruited at different frequencies. The order of recruitment of motoneurons does not obey the input resistance rule, but it is set by a combination of specific biophysical properties and the strength of synaptic currents. Our findings define different motoneuron pools in the spinal cord and the logic of their recruitment to produce locomotor behavior with increasing speed.

## Results

### Incremental recruitment of motoneuron pools

Locomotor activity was induced by electrical stimulation of descending axons and monitored by recording from peripheral motor nerves while identified primary (pMN) and secondary (sMN) motoneurons [17], pre-labeled with Rhodamine dextran, were recorded using the whole-cell patch-clamp technique (**Fig. 1a**). There was a difference in the activity of dorsal and ventral motoneurons during locomotion (**Fig. 1b**). Dorsally located motoneurons only displayed subthreshold synaptic potentials (**Fig. 1d**), while ventrally located motoneurons showed larger membrane potential oscillations and fired action potentials during some locomotor cycles (**Fig. 1e**).

Since the motor column in juvenile/adult zebrafish extends along the ventro-dorsal axis in the medial part of the spinal cord and along the medio-lateral axis in the ventral spinal cord (**Fig. 1c**), we asked if there is a difference in the activity of motoneurons located in the different parts of the motor column. At the swimming frequencies examined (4–12 Hz), primary and dorsal secondary motoneurons did not fire action potentials and received only weak synaptic potentials that were correlated with the peripheral nerve bursts (**Fig. 2a**–**f**). The peak-to-trough amplitude of the synaptic oscillations was 0.3 ± 0.1 mV (n = 8) in primary motoneurons (**Fig. 2a**–**c**) and 1.3 ± 0.2 mV (n = 14) in dorsal secondary motoneurons (**Fig. 2d**–**f**). Ventral motoneurons fired action potentials, but with a clear difference in the firing pattern between motoneurons along the medio-lateral axis of the motor column. Ventromedial motoneurons received significantly larger membrane potential oscillations (4.8 ± 0.8 mV; n = 23; $P < 0.005$) than dorsal ones that in some motoneurons (n = 9) reached the threshold for action potentials. These motoneurons fired mostly at the beginning of the swimming episode where burst frequencies were higher and only showed phasic synaptic potentials at lower frequencies (**Fig. 2g**–**i**). In contrast, ventrolateral secondary motoneurons fired continuously during the entire swimming episode and the underlying membrane potential oscillation amplitude was 15.6 ± 1.4 mV (n = 17; **Fig. 2j**–**l**). These motoneurons fired bursts of action potentials during each swimming cycle (**Fig. 2k**,**l**). Our results suggest that the motor column is organized in four different pools of motoneurons with those located ventrally mediating slow continuous swimming movements. Motoneurons in the dorsal part seem to participate only in fast movements or escape that were not elicited by the electrical stimulation used in this study [11, 26].

To assess how the synaptic potentials received by these four pools of motoneurons change with the swimming frequency, we analyzed the amplitude of the membrane potential oscillations and the instantaneous burst frequency during the entire swimming episode (**Fig.**

**3a**,**c**,**e**,**g**). The amplitude of the membrane potential oscillations in dorsal primary and secondary motoneurons was constant at frequencies below 4–6 Hz and increased linearly at higher frequencies (pMNs: **Fig. 3a**,**b**; dorsal sMNs: **Fig. 3c**,**d**). The amplitude of membrane potential oscillations was larger in ventromedial secondary motoneurons and also increased with the burst frequency (**Fig. 3e**,**f**). The amplitude of the membrane potential oscillations increased further when the frequency exceeded 4–5 Hz to reach the action potential threshold (**Fig. 3e**,**f**; see **Fig. 2h**). The ventrolateral secondary motoneurons displayed membrane potential oscillations with constant amplitude that often reached firing threshold across the whole swimming frequency range (**Fig. 3g**,**h**; see **Fig. 2k**). These results show that the membrane potential oscillations in the four pools of motoneurons display distinct properties in terms of their amplitudes and relation to the swimming frequency.

**Frequency threshold of recruitment of motoneuron pools**

The different pools of motoneurons are recruited in an incremental manner as shown by the stepwise increase in the amplitude of their membrane potential oscillations as a function of the swimming frequency (**Fig. 4a**; same data as in **Fig. 3**). Not all motoneurons were recruited at the frequencies obtained in these experiments. To estimate the frequency range at which each motoneuron pool is activated, we calculated the average slope of the increase in the amplitude of the membrane potential oscillations in relation to the swimming frequency from all motoneurons and extrapolated when it would reach 5 mV, which corresponds to the minimum oscillation amplitude seen in motoneurons firing action potentials. Ventrolateral motoneurons (n = 17) had a flat slope since the membrane potential oscillations had constant amplitudes that reached firing threshold (**Fig. 4b**). In 14 of 23 ventromedial secondary motoneurons the swimming frequency was not high enough for them to spike, we therefore analyzed the slope of the firing and non-firing motoneurons separately. The slope of the

increase in the membrane potential oscillation was steeper in the firing (n = 9) than in non-firing (n = 14) ventromedial motoneurons (**Fig. 4b**). The swimming frequency at which the non-firing motoneurons would be recruited was estimated by extrapolating the slope curve (**Fig. 4b**) and corresponded to 11 Hz. Dorsal primary (n = 8) and secondary motoneurons (n = 14) never fired action potentials during swimming episodes. Extrapolations of the slope curves (**Fig. 4b**) of these motoneurons indicate that they would be recruited at swimming frequencies of 25 Hz and 42 Hz, respectively. The motoneurons that fired action potentials were located ventrally and extended along the latero-medial axis (n = 17 ventrolateral motoneurons; n = 9 ventromedial motoneurons; **Fig. 4c**) and the mean amplitude of their membrane oscillations amplitude was 5 mV or higher (**Fig. 4d**).

To further test if the different motoneurons belong to separate pools, we used principal component analysis (PCA), a covariance-matrix-based mathematical technique, to study the variation between the different motoneurons. The relationship between the relative ventro-dorsal position of motoneurons, their size, input resistance, firing properties, and the amplitude of their membrane potential oscillations were subjected to PCA. Seven principal components were obtained of which the first two (F1 and F2) accounted for 76.8% of the observed variability. They were used to visualize the areas occupied by the different motoneurons on the principal component plane. Motoneurons belonging to the same pool were clustered with no overlap between the pools (**Fig. 4i**). These results support the existence of four pools of motoneurons that are incrementally recruited to cover the complete frequency range observed in freely swimming adult zebrafish.

**Mechanisms setting the recruitment pattern of motoneurons**

In larval zebrafish, the order of recruitment of motoneurons was correlated with their input resistance [11]. It is therefore possible that the difference in the amplitude of the membrane

potential oscillations of the four pools of motoneurons in juvenile/adult zebrafish may simply be the consequence of a gradient of their input resistance. However, we found that the input resistance of the different motoneurons was neither correlated with the amplitude of their membrane potential oscillations ($R^2 = 0.14$; **Fig. 4e**) nor with their relative ventro-dorsal position in the motor column ($R^2 = 0.17$; **Fig. 4f**) although the size of motoneuron somata increased along the ventro-dorsal axis ($R^2 = 0.74$; **Fig. 4g**). In addition there was no correlation between the resting membrane potential and the position of the different motoneurons ($R^2 = 0.2$; **Fig. 4h**). These results indicate that the recruitment pattern of the different pools of motoneurons is not the consequence of a simple input-output transformation dictated by the input resistance, but it reflects the cellular and synaptic properties of each ensemble of motoneurons.

What mechanisms underlie the differences in the membrane potential oscillations of motoneurons and the order of recruitment during swimming? Since there was no correlation between the input resistance of motoneurons and the amplitude of the membrane potential oscillations during locomotion, we then examined if there is a difference in the amplitude of the summed synaptic currents (PSCs) underlying the membrane potential oscillations. Alternating excitatory and inhibitory synaptic currents, respectively underlying on-cycle excitation and mid-cycle inhibition, were recorded from motoneurons belonging to the four pools during swimming activity (**Fig. 5**) [27]. Dorsal primary and secondary motoneurons received weak excitatory and inhibitory synaptic currents of similar amplitude (primary motoneurons: EPSCs = 5.8 ± 1.0 pA; IPSCs = 7.2 ± 1.4 pA; n = 3; **Figs. 5a**,**b** and **6a**,**e**,**f**) (secondary motoneurons: EPSCs = 7.3 ± 1.1 pA; IPSCs = 7.4 ± 2.2 pA; n = 8) (**Figs. 5c**,**d** and **6b**,**e**,**f**). Ventromedial secondary motoneurons received significantly larger excitatory and inhibitory currents than dorsal motoneurons that increased as a function of the swimming frequency ($P < 0.02$; **Figs. 5e**,**f** and **6c**). The amplitude of excitatory and inhibitory currents

was 11.8 ± 1.5 pA and 12.0 ± 2.1 pA (n = 12, **Fig. 6e–f**), respectively. Ventrolateral secondary motoneurons received larger excitatory than inhibitory currents at lower frequencies (**Figs. 5g**,**h** and **6d–f**). When the frequency exceeded 4–6 Hz, the amplitude of inhibitory currents became significantly larger than that of excitatory currents and amounted to 38.0 ± 6.3 pA and 20.8 ± 3.5 pA (n = 11), respectively (**Fig. 6e,f**). The amplitude of the excitatory (**Fig. 6g**) and inhibitory (**Fig. 6h**) currents within each motoneuron pool tended to be negatively correlated with input resistance. These results show that the amplitude of the synaptic currents underlying on-cycle excitation and mid-cycle inhibition are larger in the motoneurons recruited at slow swimming frequencies.

**Motoneuron pools with different properties**

The results above show a clear difference in the amplitude of the synaptic currents received by the different motoneuron pools. We then sought to determine if this difference is the only factor governing the recruitment pattern of the different motoneuron pools or if additional mechanisms also contribute. Therefore we examined if motoneurons belonging to different pools are equipped with specific intrinsic properties that set their firing threshold. Primary motoneurons fired action potentials only when a large depolarizing current was applied and displayed very strong adaptation (**Fig. 7a**). The minimum current required to elicit action potentials (rheobase current) in these motoneurons was 981.8 ± 94.4 pA (n = 11) and they fired only during the first 0.32 ± 0.04 s (n = 11) of the depolarizing current pulse. Dorsal secondary motoneurons also had a large rheobase current (314.8 ± 34.2 pA; n = 18) and also showed strong adaptation because they fired only during the first 0.59 ± 0.11 s of a depolarizing current pulse (**Fig. 7b**,**c**). The ventromedial secondary motoneurons had a lower rheobase current (91.7 ± 21.4 pA, n = 11; $p < 0.002$) and fired continuously during current injections with little adaptation (**Fig. 7d**,**f**). In contrast to the ventromedial secondary

motoneurons, the ventrolateral motoneurons showed short, repetitive bursts of action potentials (**Fig. 7e**,**g**). These motoneurons had a rheobase current of 73.4 ± 17.1 (n = 10), they fired several action potentials during each depolarization and subsequently hyperpolarized before they started the next burst (**Fig. 7g**). Other properties displayed by the ventrolateral motoneurons were the post-inhibitory rebound and depolarizing sag upon injection of hyperpolarizing currents (**Fig. 7h**). Thus, the different pools of motoneurons are equipped with distinct intrinsic properties that result in different firing thresholds and adaptation levels. The ventrolateral motoneurons display bursting activity, post-inhibitory rebound and sag. The combination of these properties allows these motoneurons to escape from inhibition at lower frequencies and thus fire action potentials throughout the swimming episode (see **Fig. 2k**,**l**).

**Discussion**

The spinal circuitry generates the locomotor pattern that is expressed as a coordinated activity of motoneurons controlling muscle contractions. The increase in force and speed of locomotion requires an orderly recruitment of motoneurons from those innervating slow to those innervating fast muscle fibers. Our analysis shows that motoneurons in zebrafish can be separated into four pools (**Fig. 4i**). These pools have a specific topographic location in the motor column and display characteristic cellular and synaptic properties underlying their incremental order of recruitment. The recruitment map follows a latero-medial and a ventro-dorsal order of activation and is not dependent on the input resistance of motoneurons. Secondary motoneurons located ventro-laterally are recruited at low swimming frequencies and remain active during a locomotor episode. They receive large synaptic currents and fire in bursts with post-inhibitory rebound. The number of recruited ventromedial motoneurons increases as a function of swimming frequency according to their ventro-dorsal position. The

dorsal motoneurons display strong adaptation that terminates their firing and require large current injection to reach threshold. Thus, the different pools of motoneurons possess specific synaptic and intrinsic properties that are orderly designed to confine the incremental recruitment during swimming behavior.

The size principle has classically been proposed to explain the order of recruitment of motoneurons to produce movement with increased force. The crucial property determining systematic difference in recruitment was considered to be the input resistance of motoneurons [5]. The underlying assumption is that all motoneurons receive equal synaptic inputs such that small motoneurons with less surface area, and thereby a higher input resistance, would be recruited before large ones (bigger surface with lower input resistance) [1, 3, 5, 6, 10]. However, indirect estimation of the synaptic current underlying the recruitment of motoneurons of a given pool in anaesthetized cats revealed that the current co-varied with the input resistance of motoneurons, suggesting that both properties play a role in determining the order of recruitment [8]. Our results show that the input resistance does not play a crucial role in determining the recruitment during locomotion. The important component for setting the recruitment threshold seems to be the amplitude of excitatory and inhibitory currents combined with specific membrane properties. The correlation between the size and the position of motoneurons along the ventro-dorsal axis of the spinal cord could reflect the temporal pattern of development of the different motoneurons.

In larval zebrafish the recruitment of motoneurons follows the size principle [11]. The motor column in larvae does not extend laterally and motoneurons are located medially with a ventro-dorsal organization only [16-18]. It consists of the first differentiated primary motoneurons and the dorsal secondary motoneurons born shortly thereafter [17]. The recruitment of these two pools of dorsal motoneurons is set since early developmental stages [11] and is correlated to their input resistance. However, it is not known if there is also a

gradient in their synaptic drive and intrinsic properties. In the zebrafish larvae it has been shown that old interneurons are located dorsally while newly added ones are located ventrally [15]. The ventral motoneurons could be born at later developmental stages when the animals switch to slow swimming activity. The recruitment of these late developing motoneurons is governed by their synaptic drive and intrinsic properties, but it is not correlated to their input resistance.

At later developmental stages, zebrafish acquire red muscle fibers that appear two weeks after hatching [22]. The motoneurons innervating these fibers are located in the lateral aspect of the motor column [18, 19], but it is still unclear if these "red" motoneurons are a class of neurons that appear later during development (when red muscle fibers develop). According to this arrangement, we show that the ventrolateral motoneurons innervating the late developing slow muscle fibers are activated during slow swimming activity. The increase in swimming frequency is associated with the activation of ventromedial motoneurons that are likely to innervate intermediate muscle fibers. The dorsal primary and secondary motoneurons innervating fast muscle fibers would only be activated at very high frequencies as during escape.

In our experiments the burst frequency increases gradually during a swimming episode to reach a peak and then decays gradually until the activity is terminated (see **Figs. 1e**, **2h** and **3e**). While ventrolateral sMNs are active throughout the swimming episode, the ventromedial sMNs are recruited only when the frequency exceeds a certain threshold. At the onset and the end of the episode when the frequency is low, these sMNs only exhibit subthreshold membrane potential oscillations (**Figs. 1e** and **2h**). The changes in the amplitude of the membrane potential oscillations as a function of the swimming frequency were similar during recruitment and de-recruitment. In our study, the dorsal primary and secondary motoneurons were never activated at swimming frequencies below 12 Hz. The frequency at

which these motoneurons could be recruited was estimated indirectly using the amplitude of their membrane potential oscillations and the amplitude threshold at which ventral motoneurons are recruited. We have not been able to determine if the ventral pools of motoneurons characterized in this study remain active during fast escape bends as was shown in the larval zebrafish [11, 13, 28]. Overall, it seems that during development the organization of the motor column and the principles governing motoneuron recruitment are adapted to incorporate the change from fast burst swimming in larvae to the adult pattern of slow, steady swimming movements.

The dynamics of synaptic integration in the different motoneurons can be influenced by their structure and the location of the synaptic contacts. This can impact the amplitude of the oscillations during swimming and hence the recruitment of motoneurons. It is possible that the ventrally located motoneurons recruited at lower frequencies possess persistent inward currents that can amplify the synaptic inputs as shown in other vertebrates [38]. In addition, the dorsally located motoneurons may have outward currents that dampen the synaptic integration and prevent firing of action potentials [39]. Other important factors that can contribute to setting the threshold for the different motoneurons are modulatory signals that change the input/output gain by acting on specific conductances [40-42]. In Xenopus, specific modulatory systems have been show to contribute to the maturation of swimming from a stereotyped embryonic pattern to a much more flexible output in larvae [43, 44].

We do not know how the functional identity of the different pools of motoneurons is specified during development. Developmental studies revealed that motoneurons and different sets of interneurons are generated in response to a graded extrinsic signal along the dorso-ventral axis [29-32]. In the spinal cord, a set of transcription factors controls the features of motoneurons that distinguish them from other neurons [29, 33]. These motoneurons are further segregated into motor pools that seem to be determined by Hox transcription factors [30, 33, 34].

The Nkx6 transcription factor family is important in formation of mouse spinal motoneurons [35]. In zebrafish one member of this family, *Nkx6.1,* is necessary for the development of secondary motoneurons [36] and for subtype specification of primary motoneurons [37]. Our results show that different pools of motoneurons are equipped with distinct biophysical properties that together with synaptic currents play a determinant role in setting their recruitment threshold. It is possible that specific molecular programs play a role in imposing a biophysical signature of the different pools of motoneurons. Thus far there are no specific transcriptional markers of the different secondary motoneurons. Nevertheless our results provide a functional characterization of four pools of motoneurons with distinct activity patterns during swimming. Further analysis of the ionic currents of each pool of motoneurons and the architecture of their excitatory and inhibitory synaptic drive from premotor interneurons should provide further insights into how the spinal locomotor circuitry is reconfigured to produce motor output with appropriate force and speed.

**Acknowledgements**

We thank Drs. K. Dougherty, R. Hill, S. Grillner and D. McLean for comments and critical discussion of this manuscript. This was work was funded by a grant from the Swedish Research Council, European Commission (FP7, Spinal Cord Repair), Söderberg Foundation and Karolinska Institutet. J. Gabriel and J. Ausborn received post-doctoral fellowships from the German Science Foundation.

**Author contributions**

J. P. G., J. A., K. A. and A. E. M. conceived the project and planned the experiments. J. P. G., J. A., K. A. and R. M. performed the experiments. All the authors contributed to the analysis of the data, preparation of the figures and the writing of the manuscript.

**Figure legends**

**Figure 1** Synaptic activity of identified motoneurons. (**a**) Schematic drawing of the *in vitro* brainstem/spinal cord preparation. (**b**) Overlay of DIC and fluorescence image showing the location of Rhodamine-backfilled motoneurons in the spinal cord. The scale bar indicates how soma position is measured using the normalized distance between the edge of the Mauthner (M-) axon and the dorsal edge of the spinal cord. (**c**) Transverse section of the spinal cord showing the dorso-ventral and medio-lateral organization of the motor column. (**d**) Locomotor episodes are elicited by electrical stimulation (stimulation artifact at beginning of trace) and monitored by recording from the motor nerve. The recorded dorsal secondary motoneurons (sMN, see position in (b)) display only subthreshold membrane potential oscillations. (**e**) Ventral secondary motoneurons (sMN, see position in (b)) show large membrane potential oscillations that are correlated with motor nerve bursts and reach the action potential threshold.

**Figure 2** Synaptic activity of the four different pools of motoneurons during locomotion. (**a**) Position of a recorded primary motoneuron (pMN) in an overlay of DIC and fluorescence images. (**b**) Activity of this pMN during a swimming episode. (**c**) Expanded recordings from the indicated region in (b). (**d**) Image showing the position of a dorsal secondary motoneuron (sMN). (**e**) This dorsal sMN displays subthreshold membrane potential oscillations during a swimming episode. (**f**) Expanded traces from the indicated region in (e). (**g**) Position of a ventromedial sMN close to the edge of the Mauthner axon. (**h**) This sMN shows large membrane potential oscillations that reach action potential threshold. (**i**) Expanded traces showing that this sMN often fires single action potentials during each locomotor burst. (**j**) Ventral sMN with a lateral position in the motor column. (**k**) The ventrolateral sMN is firing

continuously during the swimming episode. (**l**) This type of MN fires bursts of action potentials. Dotted lines indicate the dorsal edge of the Mauthner (M-) axon.

**Figure 3** Relationship between the motoneuron membrane potential oscillation amplitude and the swimming frequency. (**a**,**c**,**e**,**g**) Quantification of burst frequency (grey) and oscillation amplitude (colored) during a single swimming episode in a typical pMN (cyan), dorsal sMN (purple), ventromedial sMN (green) and ventrolateral sMN (red), respectively. (**b**,**d**,**f**,**h**) Graphs showing the change in oscillation amplitude plotted as a function of swimming frequency for the same episodes in pMN (cyan), dorsal sMN (purple), ventromedial sMN (green) and ventrolateral sMN (red), respectively. The data in these graphs are from the individual motoneurons shown in Figure 2.

**Figure 4** Quantification of parameters important for the recruitment of the different pools of MNs. (**a**) Incremental recruitment of four individual motoneurons at different swimming frequencies (same data and color code as in Figure 3). The dotted lines indicate the frequency at which ventrolateral and vetromedial sMNs are recruited. (**b**) Averaged slope of the increase in the membrane potential oscillations from all examined motoneurons. The pooled data from all MNs are presented as median (middle line) and quartiles (outer lines). (**c**) Percentage of MNs from each pool that fire action potentials during the swimming episodes and their relative ventro-dorsal position in the spinal cord. (**d**) Plot of the membrane potential oscillation amplitude as a function of the relative soma position. All motoneurons in which the mean amplitude of the membrane potential oscillations was above 5 mV (dotted line) fired action potentials during swimming activity. (**e**) Plot of the amplitude of membrane potential oscillation as a function of the input resistance of MNs. (**f**) Plot of the input resistance as a function of the relative ventro-dorsal position of the different MNs. (**g**)

Correlation between the soma size of MNs and their relative ventro-dorsal position in the spinal cord. (**h**) Graph of the resting membrane potential and the relative ventro-dorsal position of the different MNs along the ventro-dorsal axis in the spinal cord. (**i**) Principal component analysis using the different variables of all the recorded motoneurons showing that they fall into four pools that are separated from each other.

**Figure 5** Excitatory and inhibitory synaptic currents in the four pools of motoneurons. (**a**,**c**,**e**,**g**) Inward excitatory postsynaptic currents (EPSCs) are measured by holding the membrane potential of MNs at –65 mV, which corresponds to the reversal potential of inhibition. (**b**,**d**,**f**,**h**) Outward inhibitory postsynaptic currents (IPSCs) are measured at a holding potential of 0 mV that corresponds to the reversal potential of excitation.

**Figure 6** The amplitude of synaptic currents is correlated with the order of recruitment of MNs. (**a–d**) Graphs showing the change in the amplitude of EPSCs (filled symbols) and IPSCs (open symbols) as a function of the swimming frequency in the different types of MNs (pMN: cyan, dorsal sMN: purple, ventromedial sMN: green and ventrolateral sMN: red). (**e**) Graph of the average amplitude of EPSCs and IPSCs in individual MNs as a function of their position along the ventro-dorsal axis in the spinal cord. (**f**) Mean amplitude of excitatory and inhibitory synaptic currents in the different types of MNs (Error bars represent mean ± s.e.m.). The filled (excitatory current) and open (inhibitory current) circles represent the data points obtained from individual motoneurons recorded in different experiments. (**g**) Plot showing the mean amplitude of excitatory synaptic currents from individual MNs as a function of their input resistance. (**h**) Plot showing the mean amplitude of inhibitory synaptic currents measured in individual MNs as a function of their input resistance. Each data point

in (e), (g) and (h) correspond to a value obtained from an individual motoneuron recorded in separate experiments.

**Figure 7** Characteristic intrinsic properties of the four pools of MNs. (**a**) Primary motoneurons require large currents to reach firing threshold and display strong adaptation. (**b**) Dorsal secondary motoneurons also require somewhat large currents to reach firing threshold and show spike frequency adaptation. (**c**) Expanded trace from the region indicated with the solid bar in (b). (**d**) Ventromedial secondary motoneurons require less current to reach threshold and fire continuously during current injection. (**e**) Ventrolateral secondary motoneurons fire with bursts of action potentials in response to small current injections. (**f**) Expanded trace from the region indicated with the solid bar in (d). (**g**) Expanded trace from the region indicated with the solid bar in (**e**) showing bursting behavior. (**h**) Post-inhibitory rebound induced by hyperpolarizing current injection (upper panel). Injection of large hyperpolarizing current induces a sag potential (middle panel) followed by a burst of action potentials upon termination of the current injection (lower panel).

## Methods

### In vitro spinal cord preparation

Zebrafish (ABC and AB/Tuebingen strains) were raised and kept according to established procedures [45]. Zebrafish larval stages extend over 3–4 weeks post-fertilization and most electrophysiological studies used 3–5 days old larvae. Juvenile stages begin from week 4 post-fertilization and correspond to animals with adult morphology with fully developed fins and pigmentation. Adult stages refer to breeding animals. The animals used in this study were 6 to 10 week old (body length 18 to 25 mm) and are referred to as juvenile/adult. All experimental protocols were approved by the Animal Research Ethical Committee, Stockholm. The preparation was performed as described previously [25] with minor modifications. Zebrafish were cold-anaesthetized in a slush of frozen fish saline (containing in mM: 134 NaCl, 2.9 KCl, 2.1 $CaCl_2$, 1.2 $MgCl_2$, 10 HEPES and 10 glucose, pH 7.8 with NaOH, 290 mOsm) and eviscerated. The skull was opened and the brain was cut at the level of the midbrain. The epaxial musculature was removed up to the caudal end of the dorsal fin, leaving the musculature at the tail intact. Here, the skin was pulled away to expose the motor nerves for extracellular recordings. The vertebrae overlying the spinal cord were removed. To facilitate electrode penetration, small gashes were made in the meninges overlying the spinal cord with an etched tungsten pin. The entire spinal cord together with the hindbrain and the caudal musculature was then cut out together with the vertebral column (**Fig. 1a**) and transferred to the recording chamber. The preparation was placed on the side and fixed in place with Vaseline. A Vaseline well was made around the musculature at the tail. The saline inside of the well was replaced with α-Bungarotoxin (1 mg/ml in saline; Sigma-Aldrich), which blocks nicotinic acetylcholine receptors and effectively abolishes muscle twitches for the duration of the experiment. After ~7 minutes the α-Bungarotoxin was removed and

washed away with fresh saline. During experiments, the preparations were continuously perfused with oxygenated fish saline at room temperature.

**Motoneuron backfills**

Small crystals of the fluorescent tracer Rhodamine dextran (3000 MW, Invitrogen) were dissolved in distilled water. Etched tungsten pins were moved through the viscous dye solution so that the dye solidified on the tip. Animals were anaesthetized in Tricaine methanesulfonate (MS-222, 0.03%, Sigma-Aldrich) and placed on a glass plate. A small hole was made with an etched tungsten pin in the skin overlying the lateral myotomal musculature through which the dye-soaked pins were moved in the muscle to severe the motor axons and allow uptake of the dye. Animals were kept in fish water over night to allow for retrograde transport of the tracer and subsequently dissected as described above.

**Electrophysiology**

Extracellular recording and stimulation electrodes were pulled from borosilicate glass (1 mm outer diameter, 0.87 mm inner diameter, Harvard Apparatus) on a Flaming/Brown microelectrode puller (P-87, Sutter Instruments), broken down to the desired tip diameter (15–25 μM) and fire-polished. Extracellular recordings were performed from the motor nerves running through the intermyotomal clefts at the tail, were the musculature was left intact. Another electrode was placed dorsally on the rostral spinal cord to elicit locomotor episodes by electrical stimulation (burst duration: 1 s, pulse frequency: 10–40 Hz, pulse width: 1 ms, current amplitude: 0.3–1 mA). Extracellular signals were amplified (gain 10,000) with a differential AC amplifier (AM-Systems) and filtered with low- and high cut-off frequencies of 300 Hz and 1 kHz, respectively. Intracellular whole-cell recordings were performed from identified spinal motoneurons rostral to the peripheral nerve recording. For

intracellular recordings, electrodes were pulled from borosilicate glass (1.5 mm outer diameter, 0.87 mm inner diameter, Hilgenberg) on a vertical puller (Narishige) and filled with intracellular solution (containing in mM: 120 K-gluconate, 5 KCl, 10 HEPES, 0.0001 $CaCl_2$, 5 EGTA, 4 ATP $Mg_2$, 0.3 GTP $Na_4$, 10 phosphocreatine $Na_2$, pH 7.4 with KOH, 275 mOsm), yielding resistances of 5–8 MΩ. Cells were visualized with a microscope (Zeiss Axioskop FS Plus, Zeiss) equipped with IR-DIC optics and a CCD camera with frame grabber (Hamamatsu). Intracellular signals were amplified with a MultiClamp 700B intracellular amplifier (Axon Instruments) and low-pass filtered at 10 kHz. In current-clamp recordings, no bias current was injected. Only motoneurons that had stable membrane potentials at or below –48 mV, fired action potentials to suprathreshold depolarizations and showed minimal changes in series resistance (<5%) were included in this study.

**Measurement of soma size and position**

During the experiments we captured images that showed the outline of the soma as well as the dorsal edge of the spinal cord and the Mauthner axon (M-axon). After the experiment we analyzed the soma size and position using the measurement functions in ImageJ (available at http://rsb.info.nih.gov/ij; developed by Wayne Rasband, National Institutes of Health, Bethesda, MD). We defined a position of 1 as the dorsal edge of the spinal cord and 0 as the dorsal edge of the M-axon (**Fig. 1b**). We measured every parameter twice and used the average of the measurements. The primary and dorsal secondary motoneurons were located medially close to the central canal. Ventral motoneurons could be divided into two populations according to their soma position on the medio-lateral axis. Like the dorsal secondary and primary motoneurons, the somata of ventromedial motoneurons were located medially close to the M-axon, whereas the somata of ventrolateral secondary motoneurons were located laterally to the M-axon.

**Data analysis**

Data was digitized at 10 kHz (extracellular recordings) or 20 kHz (patch recordings) with a Digidata 1322A A/D converter (Axon Instruments) and acquired on a personal computer using pClamp software (version 9, Axon Instruments). Data analysis was performed in Spike2 (version 7, Cambridge Electronic Design). The input resistance of neurons was calculated as the slope of a regression line to the linear region of the I–V curve (membrane potentials of –90 to –60 mV), which was obtained by injection of hyperpolarizing current pulses (duration 1–2 s). To analyze the summed excitatory and inhibitory synaptic currents (PSCs), motoneurons were voltage-clamped close to the reversal potential of excitation (0 mV) or inhibition (–65 mV), respectively [27]. We analyzed the peak amplitude of the summed excitatory and inhibitory currents underlying the membrane potential oscillations and not the individual PSCs. In all cases the current traces were smoothed with a time constant of 0.01s, allowing us to detect even small changes in the current amplitude that occur in dorsal primary and secondary motoneurons. In all motoneurons the summed inward current occurred in phase with the ipsilateral motor nerve burst (**Fig. 5a**,**c**,**e**,**g**) and was alternating with the summed inhibitory current (**Fig. 5b**,**d**,**f**,**h**).

All values are given as mean ± SEM. The significance of differences of means between experimental groups and conditions was analyzed using Student's two-tailed t-test. Means were regarded as statistically significant at p-values of $<0.05$.

**References**


1. Cope, T.C. & Pinter, M.J. The Size Principle: Still Working After All These Years. *News Physiol Sci* **10**, 280-286 (1995).
2. Henneman, E. Relation between size of neurons and their susceptibility to discharge. *Science* **126**, 1345-1347 (1957).
3. Henneman, E. & Mendell, L.M. Functional organization of motoneuron pool and its inputs. in *Handbook of Physiology, Sect. 1, Vol. 2* (ed. V.E. Brooks) 423-507 (American Physiological Society, Bethesda, MD, 1981).
4. Henneman, E., Somjen, G. & Carpenter, D.O. Functional Significance of Cell Size in Spinal Motoneurons. *J Neurophysiol* **28**, 560-580 (1965).
5. Mendell, L.M. The size principle: a rule describing the recruitment of motoneurons. *J Neurophysiol* **93**, 3024-3026 (2005).
6. Kernell, D. & Zwaagstra, B. Input conductance axonal conduction velocity and cell size among hindlimb motoneurones of the cat. *Brain Res* **204**, 311-326 (1981).
7. Binder, M.D., Heckman, C.J. & Powers, R.K. Relative strengths and distributions of different sources of synaptic input to the motoneurone pool: implications for motor unit recruitment. *Adv Exp Med Biol* **508**, 207-212 (2002).
8. Heckman, C.J. & Binder, M.D. Analysis of effective synaptic currents generated by homonymous Ia afferent fibers in motoneurons of the cat. *J Neurophysiol* **60**, 1946-1966 (1988).
9. Enoka, R.M. & Stuart, D.G. Henneman's 'size principle': current issues *Trends Neurosci* **7**, 226-228 (1984).
10. Gustafsson, B. & Pinter, M.J. An investigation of threshold properties among cat spinal alpha-motoneurones. *J Physiol* **357**, 453-483 (1984).
11. McLean, D.L., Fan, J., Higashijima, S., Hale, M.E. & Fetcho, J.R. A topographic map of recruitment in spinal cord. *Nature* **446**, 71-75 (2007).
12. El Manira, A. & Grillner, S. Switching gears in the spinal cord. *Nat Neurosci* **11**, 1367-1368 (2008).
13. McLean, D.L., Masino, M.A., Koh, I.Y., Lindquist, W.B. & Fetcho, J.R. Continuous shifts in the active set of spinal interneurons during changes in locomotor speed. *Nat Neurosci* **11**, 1419-1429 (2008).

14. Fetcho, J.R. & McLean, D.L. Some principles of organization of spinal neurons underlying locomotion in zebrafish and their implications. *Ann N Y Acad Sci* **1198**, 94-104 (2010).

15. McLean, D.L. & Fetcho, J.R. Spinal interneurons differentiate sequentially from those driving the fastest swimming movements in larval zebrafish to those driving the slowest ones. *J Neurosci* **29**, 13566-13577 (2009).

16. Lewis, K.E. & Eisen, J.S. From cells to circuits: development of the zebrafish spinal cord. *Prog Neurobiol* **69**, 419-449 (2003).

17. Myers, P.Z. Spinal motoneurons of the larval zebrafish. *J Comp Neurol* **236**, 555-561 (1985).

18. van Raamsdonk, W., Mos, W., Smit-Onel, M.J., van der Laarse, W.J. & Fehres, R. The development of the spinal motor column in relation to the myotomal muscle fibers in the zebrafish (Brachydanio rerio). I. Posthatching development. *Anat Embryol* **167**, 125-139 (1983).

19. Westerfield, M., McMurray, J.V. & Eisen, J.S. Identified motoneurons and their innervation of axial muscles in the zebrafish. *J Neurosci* **6**, 2267-2277 (1986).

20. Buss, R.R. & Drapeau, P. Physiological properties of zebrafish embryonic red and white muscle fibers during early development. *J Neurophysiol* **84**, 1545-1557 (2000).

21. van Raamsdonk, W., Pool, C.W. & te Kronnie, G. Differentiation of muscle fiber types in the teleost Brachydanio rerio. *Anat Embryol* **153**, 137-155 (1978).

22. van Raamsdonk, W., van't Veer, L., Veeken, K., Heyting, C. & Pool, C.W. Differentiation of muscle fiber types in the teleost Brachydanio rerio, the zebrafish. Posthatching development. *Anat Embryol* **164**, 51-62 (1982).

23. Bone, Q., Kiceniuk, J. & Jones, D.R. On the role of the different fibre types in fish myotomes at intermediate swimming speeds. *Fishery bulletin* **76**, 691-699 (1978).

24. Johnston, I.A. On the design of fish myotomal muscles *Marine Behav Physiol* **9**, 83-98 (1983).

25. Gabriel, J.P.*, et al.* Locomotor pattern in the adult zebrafish spinal cord in vitro. *J Neurophysiol* **99**, 37-48 (2008).

26. Liu, D.W. & Westerfield, M. Function of identified motoneurones and co-ordination of primary and secondary motor systems during zebra fish swimming. *J Physiol* **403**, 73-89 (1988).

27. Gabriel, J.P.*, et al.* Serotonergic modulation of locomotion in zebrafish: endogenous release and synaptic mechanisms. *J Neurosci* **29**, 10387-10395 (2009).

28. Bhatt, D.H., McLean, D.L., Hale, M.E. & Fetcho, J.R. Grading movement strength by changes in firing intensity versus recruitment of spinal interneurons. *Neuron* **53**, 91-102 (2007).

29. Briscoe, J. & Ericson, J. Specification of neuronal fates in the ventral neural tube. *Curr Opin Neurobiol* **11**, 43-49 (2001).

30. Dasen, J.S., De Camilli, A., Wang, B., Tucker, P.W. & Jessell, T.M. Hox repertoires for motor neuron diversity and connectivity gated by a single accessory factor, FoxP1. *Cell* **134**, 304-316 (2008).

31. Goulding, M. Circuits controlling vertebrate locomotion: moving in a new direction. *Nat Rev Neurosci* **10**, 507-518 (2009).

32. Jessell, T.M. Neuronal specification in the spinal cord: inductive signals and transcriptional codes. *Nat Rev Genet* **1**, 20-29 (2000).

33. Dasen, J.S. & Jessell, T.M. Hox networks and the origins of motor neuron diversity. *Curr Top Dev Biol* **88**, 169-200 (2009).

34. Dasen, J.S., Tice, B.C., Brenner-Morton, S. & Jessell, T.M. A Hox regulatory network establishes motor neuron pool identity and target-muscle connectivity. *Cell* **123**, 477-491 (2005).

35. Vallstedt, A.*, et al.* Different levels of repressor activity assign redundant and specific roles to Nkx6 genes in motor neuron and interneuron specification. *Neuron* **31**, 743-755 (2001).

36. Cheesman, S.E., Layden, M.J., Von Ohlen, T., Doe, C.Q. & Eisen, J.S. Zebrafish and fly Nkx6 proteins have similar CNS expression patterns and regulate motoneuron formation. *Development* **131**, 5221-5232 (2004).

37. Hutchinson, S.A., Cheesman, S.E., Hale, L.A., Boone, J.Q. & Eisen, J.S. Nkx6 proteins specify one zebrafish primary motoneuron subtype by regulating late islet1 expression. *Development* **134**, 1671-1677 (2007).

38. Heckman, C.J., Lee, R.H. & Brownstone, R.M. Hyperexcitable dendrites in motoneurons and their neuromodulatory control during motor behavior. *Trends Neurosci* **26**, 688-695 (2003).

39. Johnston, D. & Narayanan, R. Active dendrites: colorful wings of the mysterious butterflies. *Trends Neurosci* **31**, 309-316 (2008).

40. Heckman, C.J., Hyngstrom, A.S. & Johnson, M.D. Active properties of motoneurone dendrites: diffuse descending neuromodulation, focused local inhibition. *J Physiol* **586**, 1225-1231 (2008).

41. El Manira, A. & Kyriakatos, A. The role of endocannabinoid signaling in motor control. *Physiology* **25**, 230-238 (2010).

42. Nanou, E.*, et al.* $Na^+$-mediated coupling between AMPA receptors and $K_{Na}$ channels shapes synaptic transmission. *Proc Natl Acad Sci U S A* **105**, 20941-20946 (2008).

43. McLean, D.L., Merrywest, S.D. & Sillar, K.T. The development of neuromodulatory systems and the maturation of motor patterns in amphibian tadpoles. *Brain Res Bull* **53**, 595-603 (2000).

44. Sillar, K.T., Reith, C.A. & McDearmid, J.R. Development and aminergic neuromodulation of a spinal locomotor network controlling swimming in Xenopus larvae. *Ann N Y Acad Sci* **860**, 318-332 (1998).

45. Westerfield, M. *The zebrafish book. A guide for the laboratory use of the zebrafish (Danio rerio)* (University of Oregon Press, Eugene, 2000).

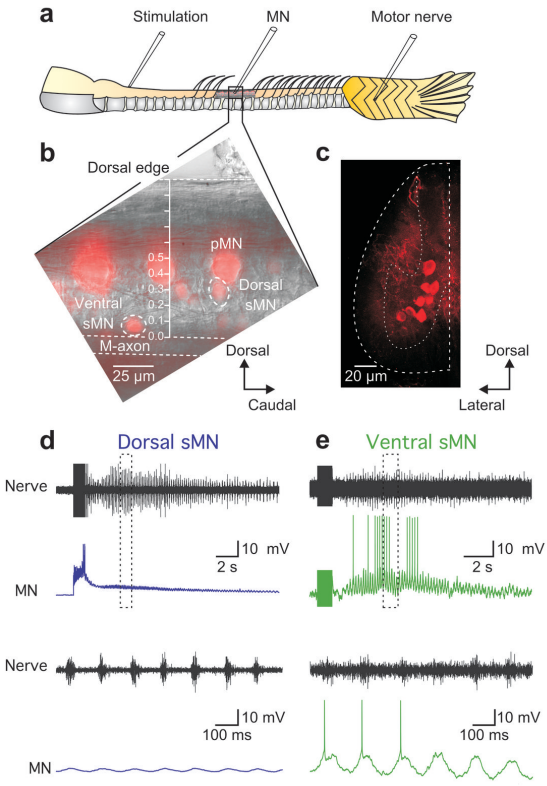
a
Stimulation
MN
Motor nerve
b
Dorsal edge
pMN
Dorsal sMN
Ventral sMN
M-axon
25 µm
Dorsal
Caudal
c
20 µm
Dorsal
Lateral
d
Dorsal sMN
Nerve
10 mV
2 s
MN
10 mV
100 ms
e
Ventral sMN
10 mV
2 s
10 mV
100 ms

Fig. 1

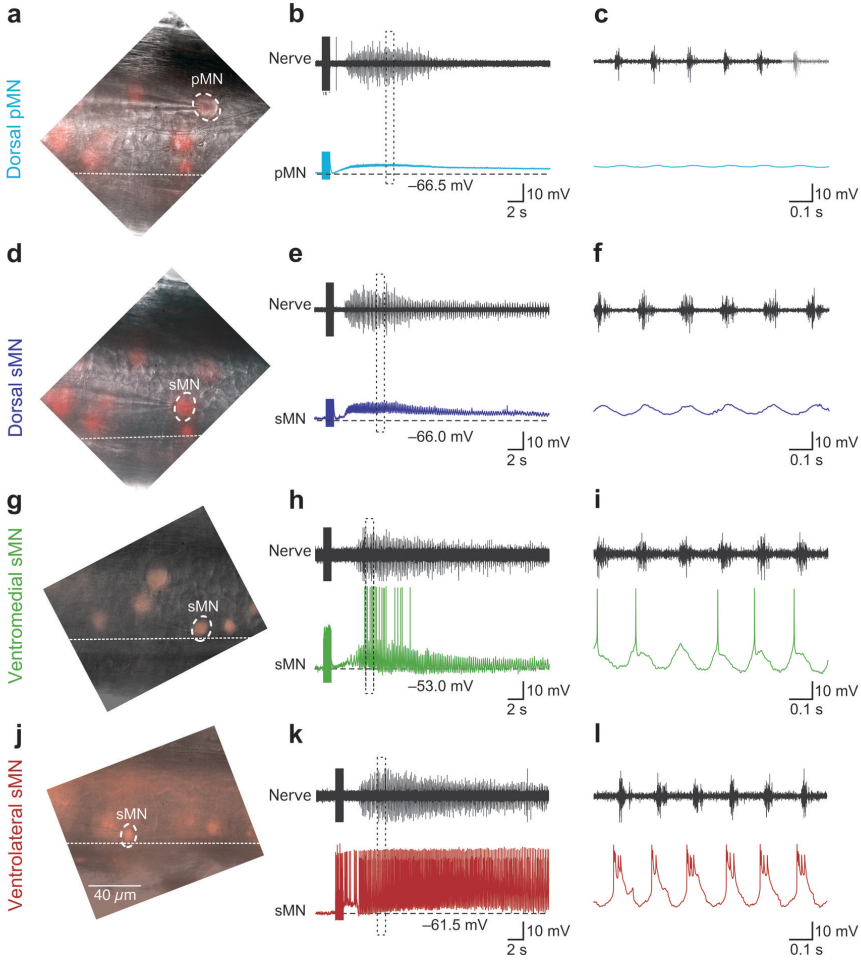
a
Dorsal pMN
pMN
b
Nerve
pMN
–66.5 mV
10 mV
2 s
c
10 mV
0.1 s
d
Dorsal sMN
sMN
e
Nerve
sMN
–66.0 mV
10 mV
2 s
f
10 mV
0.1 s
g
Ventromedial sMN
sMN
h
Nerve
sMN
–53.0 mV
10 mV
2 s
i
10 mV
0.1 s
j
Ventrolateral sMN
sMN
40 μm
k
Nerve
sMN
–61.5 mV
10 mV
2 s
l
10 mV
0.1 s

Fig. 2

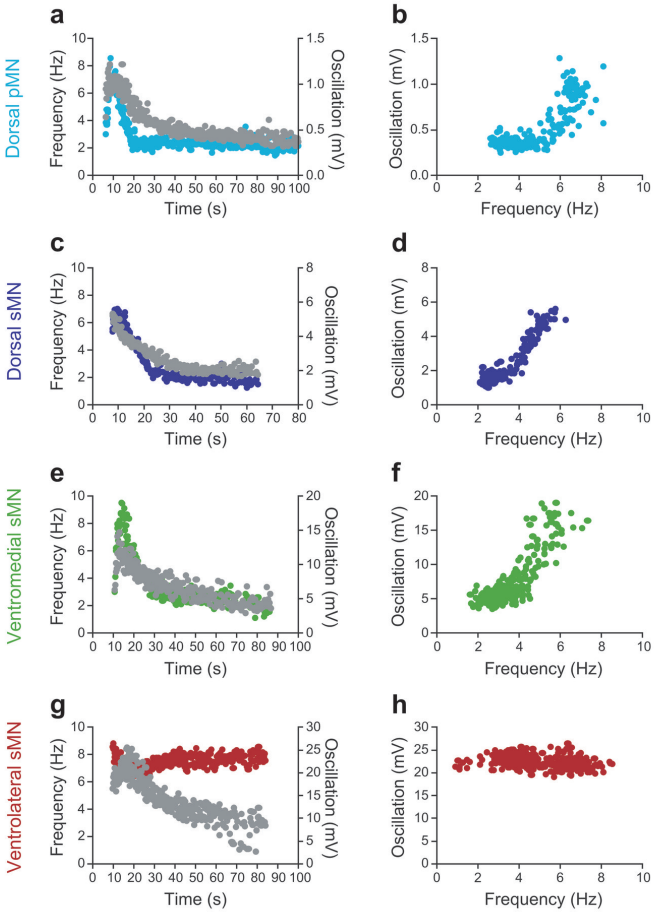
a
b
c
d
e
f
g
h
Dorsal pMN
Dorsal sMN
Ventromedial sMN
Ventrolateral sMN
Frequency (Hz)
Oscillation (mV)
Time (s)
Frequency (Hz)

Fig. 3

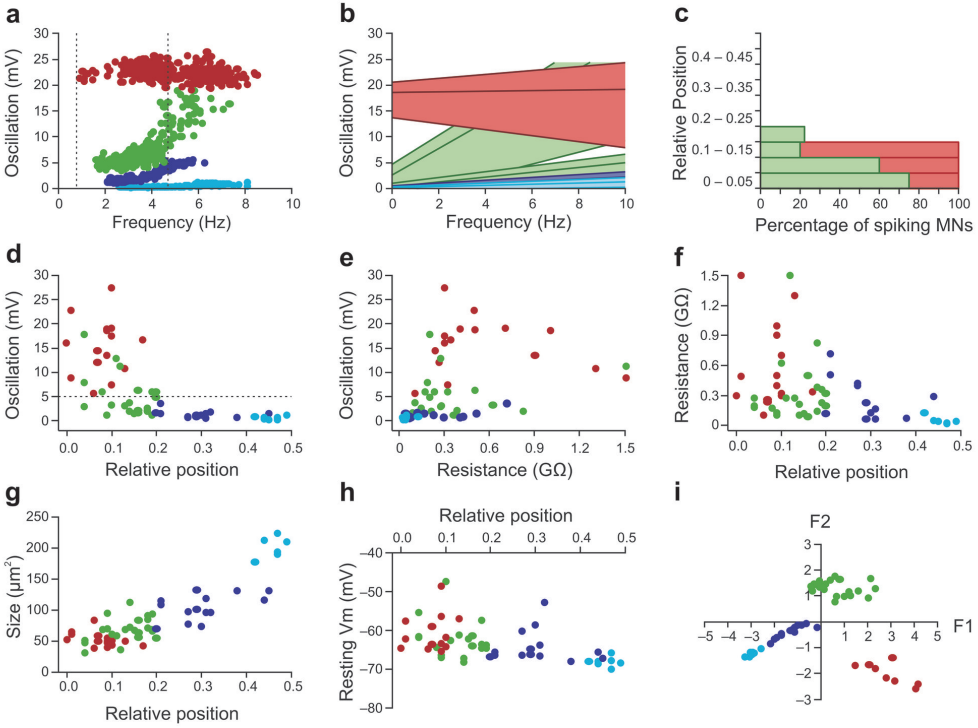
a
Oscillation (mV)
Frequency (Hz)
b
Oscillation (mV)
Frequency (Hz)
c
Relative Position
0.4 – 0.45
0.3 – 0.35
0.2 – 0.25
0.1 – 0.15
0 – 0.05
Percentage of spiking MNs
d
Oscillation (mV)
Relative position
e
Oscillation (mV)
Resistance (GΩ)
f
Resistance (GΩ)
Relative position
g
Size (μm²)
Relative position
h
Relative position
Resting Vm (mV)
i
F2
F1

Fig. 4

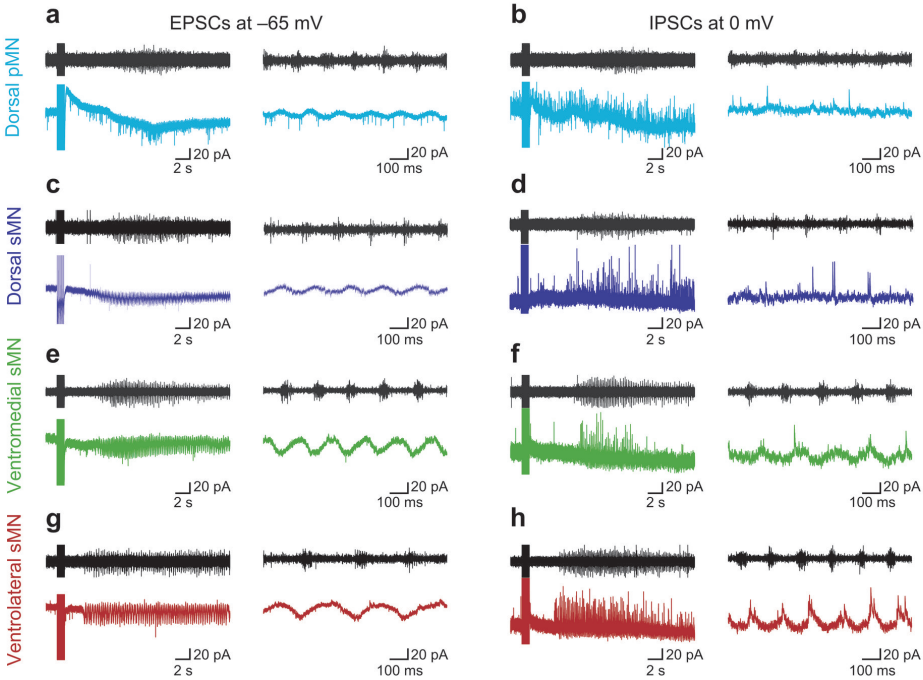
a
EPSCs at –65 mV
b
IPSCs at 0 mV
Dorsal pMN
c
Dorsal sMN
d
e
Ventromedial sMN
f
g
Ventrolateral sMN
h
20 pA
2 s
20 pA
100 ms

Fig. 5

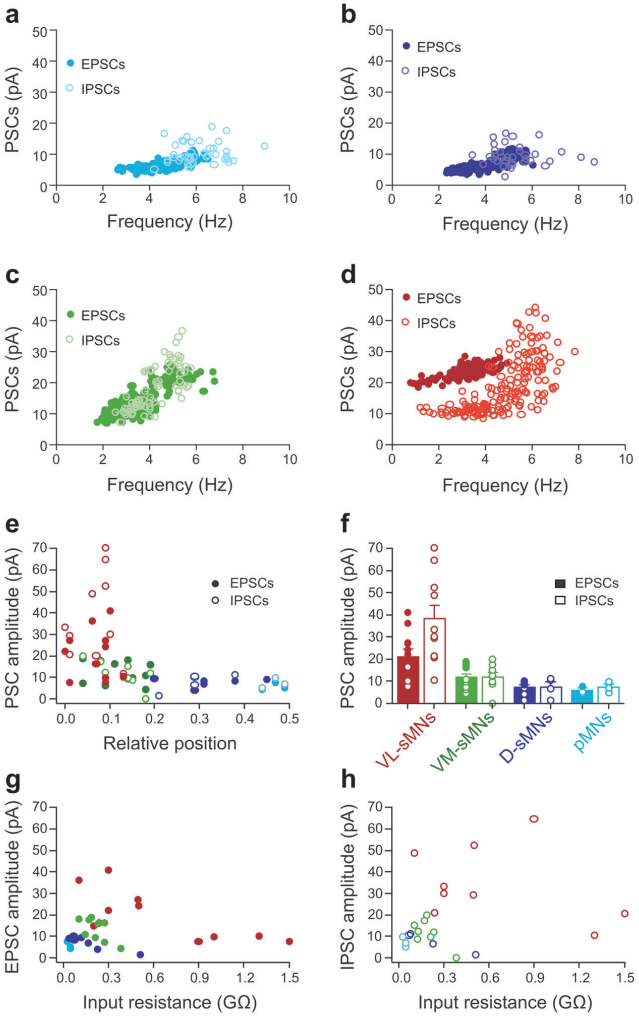
a
b
c
d
e
f
g
h
PSCs (pA)
Frequency (Hz)
EPSCs
IPSCs
PSC amplitude (pA)
Relative position
VL-sMNs
VM-sMNs
D-sMNs
pMNs
EPSC amplitude (pA)
IPSC amplitude (pA)
Input resistance (GΩ)

Fig. 6

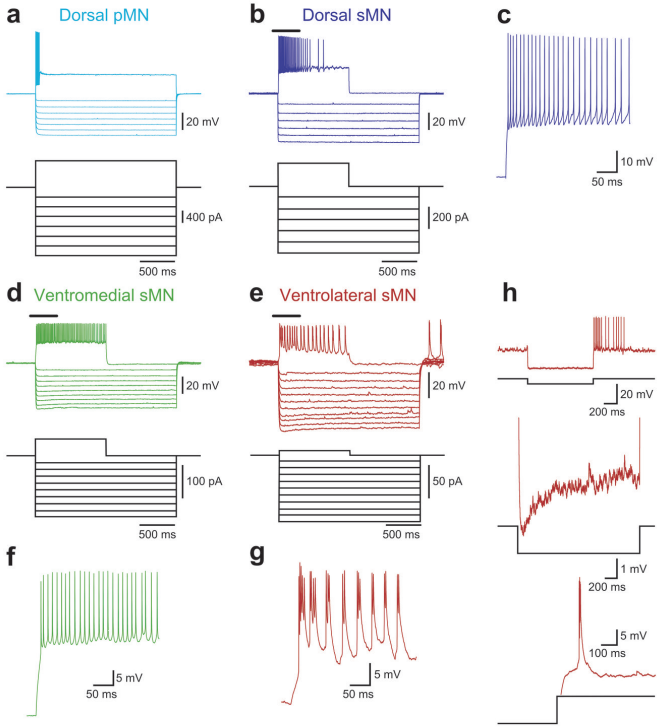
a
Dorsal pMN
20 mV
400 pA
500 ms
b
Dorsal sMN
20 mV
200 pA
500 ms
c
10 mV
50 ms
d
Ventromedial sMN
20 mV
100 pA
500 ms
e
Ventrolateral sMN
20 mV
50 pA
500 ms
h
20 mV
200 ms
1 mV
200 ms
5 mV
100 ms
f
5 mV
50 ms
g
5 mV
50 ms

Fig. 7